Excited State Dynamics of a Substituted Fluorene Derivative. The Central Role of Hydrogen Bonding Interactions with the Solvent

Briana A. Capistran,¹ Stephen H. Yuwono,¹ Mehdi Moemeni,¹ Soham Maity,¹ Aria Vahdani,¹ Babak Borhan,¹ James E. Jackson,¹ Piotr Piecuch,^{1,2} Marcos Dantus,^{1,2} and G. J. Blanchard^{1,*}

Abstract

Substituted fluorene structures have demonstrated unusual photochemical properties. Previous reports on the substituted fluorene Schiff Base **FR0**-SB demonstrated super photobase behavior with ΔpK_b of ~15 on photoexcitation. In an effort to understand the basis for this unusual behavior, we have examined the electronic structure and relaxation dynamics of the structural precursor of **FR0**-SB, the aldehyde **FR0**, in protic and aprotic solvents using time-resolved fluorescence spectroscopy and quantum chemical calculations. The calculations show three excited singlet states in relatively close energetic proximity. The spectroscopic data are consistent with relaxation dynamics from these electronic states that depend on the presence and concentration of solvent hydroxyl functionality. These results underscore the central role of solvent hydrogen-bonding to the **FR0** aldehyde oxygen in mediating the relaxation dynamics within this molecule.

¹ Department of Chemistry, Michigan State University, East Lansing, MI 48824, USA

² Department of Physics and Astronomy, Michigan State University, East Lansing, MI 48824, USA

^{*} Author to whom correspondence should be addressed. Email: blanchard@chemistry.msu.edu. Tel: +1 517 353 1105

Introduction

Chemical reactions are typically performed in the liquid phase or at the interface between phases with reactants in their ground states. Under such conditions there is little opportunity to control the temporal or spatial extent of the reaction. While photochemical reactions are among the best candidates for such controls by requiring excitation of one reactant to initiate the reaction, their use has historically been limited. Therefore, by gaining broader utility in photochemical reactions one affords new opportunities for temporal and spatial control of reaction chemistry, properties that are central to the emerging fields of precision chemistry and high-speed chemical sensing.

Essentially all chemical reactions are either acid-base (proton transfer) or redox (electron transfer) reactions. The ability to alter the acidity or basicity of certain compounds through photoexcitation has been explored extensively for photoacids, which are photoactivated proton donors, ^{1,2} but the development of their photobase counterparts, which are able to abstract available protons from their local environment upon photoexcitation, has been much more limited. Recently, we have focused on the design and characterization of the super photobase **FR0**-SB³⁻⁶ that is capable of exhibiting a remarkable increase in K_b of 15 orders of magnitude (or $\Delta p K_b \sim 15$) upon photoexcitation. The behavior of **FR0**-SB (Fig. 1a) in protic and aprotic media has been reported recently, ⁴⁻⁶ providing fundamental insight into the proton abstraction reaction that occurs in protic solvents. Among the issues that require further investigation is the chemical structural basis for such a large change in the basicity of the imine nitrogen upon photoexcitation. In an effort to understand more completely the structural properties that lead to super photobase behavior, we have examined the excited state properties of the aldehyde precursor of **FR0**-SB, namely, **FR0** (Fig. 1b).

A comprehensive understanding of the reactivity and excited-state population relaxation dynamics of such precursor molecules is a key step toward the rational design of super photobases with controlled properties for specific applications. In this work, we report on the reactivity and excited-state relaxation dynamics of the **FR0** precursor molecule in protic and aprotic solvent media using steady-state and time-resolved spectroscopy in conjunction with quantum chemical computational results.

The spectroscopic properties of the super photobase FR0-SB lend themselves to the study of its photoreactivity. Emission bands for unprotonated and protonated forms of the photoexcited Schiff base FR0-SB* are well resolved, and the time-evolution of those band intensities provides direct insight into solvent proton abstraction by FR0-SB*. The data reported here for FR0 also exhibit spectral dynamics, although resolution of individual bands is not as facile. The emission spectrum of FR0 exhibits time-dependent changes in band shape and position in protic solvents, suggesting a significant role of the FR0 chromophore structure in the unusual photobase behavior of the corresponding Schiff base. We report on the presence of overlapped electronic singlet state manifolds within the FR0 emission band and population exchange between those singlet states in protic solvents. The excited-state relaxation dynamics of FR0 depend on the identity of the (protic) solvent. Spectral reconstruction from the time-resolved emission data reveals the details of band evolution and demonstrates that the relaxation dynamics of the FR0 precursor molecule are mediated by hydrogen-bonding interactions between FR0 and the surrounding solvent medium.

Experimental Methods

Materials. n-Propanol (99.7%, anhydrous), n-pentanol (\geq 99%, ACS grade), and dimethyl sulfoxide (DMSO, \geq 99.9%, anhydrous) were all purchased from Sigma-Aldrich and used as

received. *n*-Pentanol, which was not available in anhydrous form, was stored over molecular sieves (Type 3A).

Synthesis of FR0. The synthesis of FR0 followed the procedure reported previously^{3, 7} and is described briefly here. The synthesis commenced with fluorene, which was converted to 2bromofluorene by treating with N-bromosuccinimide in propylene carbonate at room temperature. Dimethylation of the C9 position was accomplished with treatment of the brominated fluorene with excess iodomethane in the presence of NaOH. Fuming nitric acid was used for nitration of the nonbrominated aryl ring to yield 2-bromo-9,9-dimethyl-7-nitro-9H-fluorene. Subsequent reduction of the nitro group with iron powder suspended in an aqueous ammonium chloride solution provided the corresponding amine. The resulting product was heated with ethyl iodide and potassium carbonate generating the diethyl amino substituent. Metal/halogen exchange promoted by the addition of n-BuLi, followed by addition of DMF led to the formation of FR0. Purification of the crude on a silica-gel column (hexane/ethyl acetate eluant) provided the title compound as a yellow solid. $^{1}\text{H-NMR}$ (500 MHz, CDCl₃), δ (ppm) = 9.98 (d, J = 0.8 7.90 – 7.85 (m, 1H), 7.78 (dt, J1 = 7.8 Hz, J2 = 1.1 Hz, 1H), 7.68 - 7.59 (m, 2H), 6.73 - 6.66 (m, 2H), 3.46(q, J = 7.1 Hz, 4H), 1.50 (s, 6H), 1.30 - 1.20 (m, 7H). ¹³C-NMR (125 MHz, CDCl₃): δ (ppm) = 192.05, 157.33, 153.19, 148.99, 146.90, 133.41, 131.27, 125.20, 122.47, 122.35, 118.12, 110.87, 105.06, 46.62, 44.71, 27.24, 12.59.

The compound was stored in ethanol (1 mM). To prepare samples of **FR0** in each solvent, aliquots of **FR0** were brought to dryness using nitrogen and reconstituted with the solvent system to be studied at a concentration appropriate for the measurement, typically ca. 5×10^{-6} M.

Steady-State Emission Spectroscopy. Emission spectra for FR0 in each of the solvents were collected using a Hitachi F-4500 fluorescence spectrometer and Spex Fluorolog 3 emission

spectrometer. Quartz cuvettes (1 cm) were used for all measurements and spectra were acquired using an excitation wavelength of 440 nm, with excitation and emission spectral resolution of 1 nm.

Time-Resolved Fluorescence Spectroscopy. Time-resolved fluorescence measurements were collected using a time-correlated single photon counting (TCSPC) instrument that has been described in detail elsewhere, 8-9 so we provide only a brief summary here. The light source is a continuous-wave passively mode-locked Nd:YVO₄ laser (Spectra Physics Vanguard), that produces 13 ps pulses at 1064 nm (80 MHz repetition rate). The output of this laser was at the second harmonic (532 nm) and the third harmonic (355 nm), with 2.5 W average power at both wavelengths, with the same pulse duration. For the experiments reported here, the cavity-dumped dye laser (Coherent 702-2) was excited by the third harmonic output of the pump laser. The dye used was Stilbene 420 (Exciton) and the dye laser output at 440 nm was 5 ps full-width at halfmaximum (FWHM) pulses at a repetition rate of 4 MHz. The pulses from the dye laser were divided with approximately half going to a reference channel diode (Becker and Hickl PHD-400-N) and the remaining light going to the sample. The vertically polarized excitation light was focused on the sample cuvette and a reflecting microscope objective (40X, Ealing) was used to collect emission. The collected emission was passed through a polarization-selective beamsplitter and sent to two identical detection channels. Each detection channel had a subtractive double monochromator (Spectral Products CM-112) and a microchannel plate photomultiplier tube (PMT) detector (Hamamatsu R3809U-50). Signals from each detector were sent to TCSPC detection electronics (Becker & Hickl SPC-132). Typical instrument response function for this system is ca. 35 ps FWHM. The TCSPC acquisition electronics, PMT bias and monochromator wavelengths were controlled using a computer program written in-house using LabVIEW®

(National Instruments) software. For these experiments, time-resolved fluorescence data were acquired from 470 nm to 620 nm, in 10 nm increments. All raw time-domain data were exported to Microsoft Excel (Microsoft Office 365, Microsoft Corporation, Redmond, WA). Data analysis, including extraction of fluorescence lifetime decay constants and band fitting, was performed using Microcal Origin (OriginPro 9.0, OriginLab Corporation, Northampton, MA).

Computational Details

The quantum chemistry calculations performed in this work were based on the computational protocol that has been described in detail in our earlier work.⁴ We started by optimizing the geometry of the isolated **FR0** chromophore in its ground electronic state S_0 using the Kohn–Sham¹⁰ formulation of density functional theory,¹¹ where we employed the CAM-B3LYP¹² functional and the 6-31+G* basis set.¹³⁻¹⁵ Subsequently, we used the equation-of-motion (EOM)¹⁶ extension of coupled-cluster (CC)¹⁷ theory to excited electronic states to determine the vertical excitation energies characterizing the transitions from the ground state (S_0) to the four lowest excited singlet states (S_n , n = 1-4) of the **FR0** molecule using the composite formula

$$\omega_n^{\text{(EOMCC)}} = \omega_n^{\text{(EOMCCSD/6-31+G*)}} + [\omega_n^{(\delta-\text{CR-EOMCC}(2,3)/6-31G)} - \omega_n^{\text{(EOMCCSD/6-31G)}}]. \tag{1}$$

The first term on the right-hand side of Eq. 1 denotes the vertical excitation energy obtained using the EOM extension of the CC method with singles and doubles (CCSD),¹⁸ designated as EOMCCSD,¹⁶ in conjunction with the 6-31+G* basis set. The next two terms on the right-hand side of Eq. 1 correct the EOMCCSD/6-31+G* results for the higher-order many-electron correlation effects due to triple excitations, represented in this work by the δ-CR-EOMCC(2,3) approach,¹⁹ computed at the smaller 6-31G basis set.¹³ We also used the CCSD/6-31+G* and EOMCCSD/6-31+G* one-electron reduced density matrices to determine the Mulliken atomic

charges, permanent dipole moments, and total electron densities characterizing the ground and excited states, as well as the transition dipole moments and oscillator strengths associated with the vertical $S_m \to S_n$ excitations to the lowest four excited singlet states of **FR0**.

All electronic structure calculations for the **FR0** molecule reported in this work were performed using GAMESS.²⁰⁻²¹ The relevant CCSD, EOMCCSD, and δ-CR-EOMCC(2,3) computations using the restricted Hartree–Fock (RHF) determinant as a reference and the corresponding left-eigenstate CCSD and EOMCCSD calculations, required to obtain the triples corrections of δ-CR-EOMCC(2,3) and the one-electron properties of interest, were performed using the CC/EOMCC routines developed by the Piecuch group,²²⁻²⁵ which form part of the GAMESS code. In all the post-RHF calculations, the core orbitals corresponding to the 1s shells of the C, N, and O atoms were kept frozen. In the calculations employing the 6-31+G* basis set, we used the spherical d-type polarization functions. We used the VMD software²⁶ to visualize the **FR0** species.

Results and Discussion

As mentioned in the Introduction, the super photobase **FR0**-SB exhibits an anomalously large change in its excited state pK_b^{4-5} and among the issues that remain to be resolved is the role that the fluorene derivative chromophore structure plays in producing this behavior. In this work, we investigate the precursor to **FR0**-SB, the aldehyde **FR0** (Fig. 1b), which exhibits unusual fluorescence relaxation dynamics in protic solvents. We present the time-resolved spectra for **FR0** in *n*-propanol (Fig. 2a), *n*-pentanol (Fig. 2b) and DMSO (Fig. 2c). These spectra were extracted from time-domain experimental data with integrated emission intensity normalized to the steady-state fluorescence spectrum.

For the time-resolved spectral evolution seen with **FR0**-SB, there were well resolved emission bands corresponding to unprotonated and protonated species,⁴⁻⁶ but for **FR0** there is no corresponding imine and, consequently, no analogous spectrally resolved features. It is thus important to consider first whether the data shown in Figs. 2a and 2b represent spectral shifts of a single electronic state in time or the evolution of populations in multiple spectrally overlapped bands. There are several factors that point to the latter explanation being correct.

There is a substantial volume of literature related to spectral evolution and its relationship to solvation dynamics.²⁷⁻³¹ One of the most well-known examples is the probe molecule Coumarin 153, which has been studied extensively and found to exhibit a time-resolved fluorescence Stokesshift²⁸⁻³⁴ that is mediated by solvent relaxation.^{27, 35} The data for the time-resolved Stokes-shift seen for Coumarin 153 resemble, at least qualitatively, the results shown in Figs. 2a and 2b. The observed spectral relaxation for Coumarin 153 correlates with the solvent Debye relaxation time at the scale of ca. 50-100 ps, which is somewhat shorter than that of the spectral shift we observe but not necessarily at odds with the relaxation times in normal alcohols.³⁶ More importantly, the solvent-relaxation model presumes that the spectral dynamics are mediated by relaxation along a featureless reaction coordinate that is determined by the time required for the solvent surrounding the dipolar excited state to accommodate to the change in dipole moment orientation and magnitude resulting from excitation. If other intramolecular processes such as IVR or relaxation between multiple electronic state manifolds can be shown to contribute, then the spectral relaxation process cannot be assigned to solvent relaxation alone. There are several pieces of information, both experimental and computational, that point to the spectral dynamics we report here being understood in the context of intramolecular relaxation dynamics that are mediated by specific intermolecular interactions. In addition to the analysis provided in the following sections, we have

taken the time-resolved emission data at several different wavelengths across the **FR0** emission band and have extracted the rotational diffusion time constants from different emission wavelengths. The reorientation time of **FR0** in the alcohols exhibits a measurable wavelength-dependence. We will return to a more thorough discussion of this point below, but wavelength-dependent reorientation times require the existence of multiple excited electronic states, each with a finite radiative lifetime. We assert that the correct analysis of the data involves multiple electronic states rather than the temporal evolution along a solvent-mediated relaxation coordinate for a single electronic state.

Computational chemistry has demonstrated its importance in understanding molecular-scale phenomena and spectroscopic dynamics of the super photobase FR0-SB.⁴⁻⁶ We have applied the protocol described in the Computational Details section to investigate the electronic structures of the ground state S₀ and four lowest singlet excited states S₁-S₄ of FR0 and the results of those calculations reveal several interesting features that assist in our understanding of the complex spectral dynamics shown in Fig. 2. The $S_0 \rightarrow S_n$ vertical excitation energies and permanent dipole moments of the S₁-S₄ states of FR0 are reported in Table 1, while the transition dipole moments and oscillator strengths characterizing the $S_m \to S_n$ vertical excitations to these excited states are reported in Table 2. The Mulliken charges in the ground S₀ and excited S₁, S₂ and S₃ states are shown in Fig. 3 and the comparison of the magnitude and direction of the permanent dipole moments in each state, along with the electron density difference characterizing the $S_0 \rightarrow S_n$ (n =1–3) vertical excitations, are shown in Fig. 4. There are several interesting points that stem from these results. The first is that, as shown in Table 1, there are three excited electronic singlet states in relatively close energetic proximity, S_1-S_3 , which suggest facile population relaxation from S_3 to S_2 or S_1 and from S_2 to S_1 . The second important result of these calculations is that the S_0 , S_1

and S_3 states all exhibit relatively similar electron densities for the aldehyde moiety, with the carbonyl oxygen carrying a Mulliken charge of ca. -0.4, and, not surprisingly, the dipole moments are oriented along similar axes. The S_2 state, however, exhibits a significantly different electron density distribution for the aldehyde group, with the carbonyl oxygen exhibiting a Mulliken charge of ca. -0.1 and the aldehyde carbon being substantially more negative (see Fig. 3). These differences in Mulliken charges are reflected in the relatively small permanent dipole moment in S_2 relative to that seen for the other electronic states (cf. Table 1 and Fig. 4). These findings are consistent with our experimental data, as discussed below.

The existence of several excited electronic states in close energetic proximity combined with the unusual spectral dynamics in alcohols suggests that these experimental results are accounted for by population relaxation between the excited electronic states and radiative relaxation from each state, rather than the temporal evolution of a single band. We propose a kinetic model that is consistent with the observed spectroscopic behavior (Fig. 5), as defined below:

$$\frac{dS_3}{dt} = -(k_{30} + k_{31} + k_{32})S_3,$$

$$\frac{dS_2}{dt} = k_{32}S_3 - (k_{20} + k_{21})S_2, \text{ and}$$
 (2)

$$\frac{dS_1}{dt} = k_{31}S_3 + k_{21}S_2 - k_{10}S_1.$$

In this model the transitions associated with k_{30} , k_{20} and k_{10} are all considered to be radiative and the relaxation phenomena described by k_{32} , k_{31} and k_{21} are non-radiative. We also consider the excitation to be instantaneous and indicated by the quantity $\delta(t)$, which is taken to indicate a short laser pulse. The temporal evolution of the populations of each state is given by

$$S_3(t) = S_3(0) \exp(-(k_{30} + k_{31} + k_{32})t),$$

$$S_2(t) = \left(S_2(0) + \int_0^t k_{32} \exp(k_{20} + k_{21})x \cdot S_3(x) dx\right) \exp(-(k_{20} + k_{21})t), \text{ and}$$
(3)

$$S_1(t) = \left(S_1(0) + \int_0^t \exp(k_{10}x) \cdot \left(k_{21}S_2(x) + k_{31}S_3(x)dx\right)\right) \exp(-k_{10}t).$$

With the time-resolved intensities of the three bands determined, it is possible to estimate the rate constants for the model shown in Fig. 5 and Eqs. 2. Comparing the kinetic model described above to experimental data is not as straightforward as fitting individual time-resolved fluorescence intensity decays at specific wavelengths. As noted above, the emission spectrum of **FR0** is broad and relatively featureless, and the presence of multiple radiative decays will be complicated by spectral overlap of unresolved bands. We have fitted the steady-state emission spectra of **FR0** in the solvents used in this work to three Gaussian bands (Fig. 6). Using these fitted band energies, we have taken time-slices of the normalized time-domain data and have fitted those time-resolved spectra to determine the band intensities of each of the fitted bands as a function of time. In that manner we extract the time-evolution of each of the three spectral features. Based on the transition energies, we assign the highest, intermediate, and lowest energy bands to be the $S_3 \to S_0$, $S_2 \to S_0$, and $S_1 \to S_0$ emissions, respectively. While not without precedent, it is noteworthy that $S_2 \to S_0$ emission appears prominently, 37-38 especially in light of the calculated transition dipole moments and oscillator strengths (Table 2). This issue remains under investigation.

In addition to the complexities associated with spectral overlap and limited signal-to-noise ratio, extracting the rate constants from the time-resolved spectral data is inherently under-determined because we are trying to evaluate six rate constants using the decay profiles of three bands. For this reason, we apply the following constraints to place physically realistic estimates

on our estimated rate constants. The first constraint is that all rate constants must be greater than or equal to zero. The second constraint is that the lifetime of the first excited singlet state, S_1 , is on the order of several nanoseconds (*i.e.*, $k_{10} \le 10^9$). With these basic constraints, we have used a Monte Carlo fitting routine (coded in-house) to estimate the rate constants for the temporal evolution of the fitted emission bands (Table 3). The fits of Eqs. 2 to the experimental data using the rate constants in Table 2 are shown in Fig. 7. We note that the spectral dynamics we have discussed to this point are seen in protic solvents but not in aprotic solvents, such as DMSO. Based on this information we assert that the spectral dynamics we observe are associated with hydrogen bonding between solvent molecules and the **FR0** chromophore.

While the ability of the solvent to form hydrogen bond with **FR0** is related to the observed spectral dynamics, it is important to consider what the dominant factor in that dependence is. Based on the data shown in Table 2 it is not possible to determine whether the observed solvent-dependent changes in rate constants are dependent primarily on the hydroxyl concentration or the viscosity of the solvent. An alternative way to phrase this uncertainty is whether or not large amplitude molecular motion, such as rotation of the diethylamino moiety, mediates the observed spectral relaxation dynamics. We can resolve this issue experimentally.

We performed a series of measurements in binary solvent systems of DMSO and n-propanol in which the amount of each solvent is controlled. The reason for the choice of DMSO and n-propanol as the two solvents is twofold: first, the spectral dynamics seen in n-propanol are not seen in DMSO, and second, the two solvents have essentially the same bulk viscosity ($\eta_{DMSO} = 1.99 \text{ cP}$ and $\eta_{n\text{-propanol}} = 1.94 \text{ cP}$). Thus, the binary solvent systems used will allow control over hydroxyl group concentration ([OH]) under constant viscosity conditions. We report the fitted rate constants for 100%, 75%, 50% and 25% n-propanol in Table 4. These data are shown graphically

in Fig. 8 and they reveal several interesting features. Specifically, the rate constants k_{32} and k_{31} decrease with increasing [OH], k_{20} increases with [OH] and the rate constants k_{30} , k_{21} and k_{10} are independent of [OH]. One conclusion from these data is that the spectral dynamics we observe are associated with [OH] and not large amplitude molecular motion. This finding is consistent with the computational results (Fig. 3) showing no significant accumulation of positive charge on the amino nitrogen in any of the excited electronic states when compared to the ground state, precluding any contribution from charge-separated species.

The [OH]-dependence of k_{32} and k_{31} indicates that the formation of a hydrogen bond between FR0 and the solvent alcohol mediates intramolecular relaxation from S₃ to both S₂ and S₁. The formation of a hydrogen bond between **FR0** and an alcohol does not, however, influence k_{30} or k_{10} . It is possible that the formation of a hydrogen bond between the alcohol proton and the **FR0** carbonyl oxygen serves to reduce the dipole moment of the excited FR0, thereby diminishing the dipolar coupling between the excited FR0 and DMSO. This explanation is based on the observation that k_{3x} (x = 0-2) is faster than we can measure with our instrumentation in DMSO, implying either facile quenching of S₃ by DMSO or dipolar enhancement of internal conversion in **FR0**. The observation that k_{20} increases with [OH] is consistent with the formation of the hydrogen bond between the alcohol proton and FR0 carbonyl oxygen in S2 increasing the magnitude of the dipole moment relative to the gas phase value, similar to our previous observations in the computations of FR0-SB in its S₀ and S₁ states hydrogen bonded to alcohol solvent molecules, 6 enhancing dipolar interactions between DMSO and FR0 in its S_2 state. An implication of these explanations for our experimental observations is that there may be observable state-dependent solvent-interactions with the **FR0** chromophore.

We can test this hypothesis by examining the rotational diffusion behavior of **FR0** in *n*-propanol, *n*-pentanol, and DMSO as a function of emission wavelength, which we show in Table 5. The fluorescence anisotropy and lifetime components data in Table 5 demonstrate state-dependent reorientation dynamics for **FR0** in protic solvents and state-independent reorientation dynamics in DMSO. The reorientation time constants for **FR0** in *n*-propanol and *n*-pentanol exhibit three regions, with the reorientation time being fastest in S₃ and slowest in S₂, with S₁ reorientation being intermediate in value. There is no state-dependence for **FR0** in DMSO outside the experimental uncertainty, consistent with rapid relaxation of higher excited singlet states in this dipolar solvent. While it may be tempting to extract more quantitative information from these data relating to solvent association between **FR0** and the alcohols, there are several factors (*e.g.*, local heating, hydrogen bond lifetime in each state) that we cannot determine with sufficient certainty to allow further interpretation. We note that it is unusual for a molecule to exhibit significant radiative lifetimes for each of three singlet electronic states and this anomalous behavior invites further investigation.

The spectral dynamics data, taken in conjunction with the wavelength-dependent reorientation data, support the validity of our interpretation of the dynamics data in the context of multiple emissive states relaxing at different rates rather than as a single electronic state exhibiting a spectral shift. The computational results indicate that the S_2 state is characterized by an electron density distribution that differs significantly from the electron density distributions seen in S_1 and S_3 (Figs. 3 and 4). The singlet state S_2 is characterized by a permanent dipole moment that is substantially smaller in magnitude than that for S_1 and S_3 (Fig. 3), since the change in total electronic density associated with the $S_0 \rightarrow S_2$ transition is localized significantly on the aldehyde carbonyl functionality (Fig. 4). The rate constant data and its dependence on the concentration of [OH] in

solution points to the importance of dipole-dipole interactions in determining coupling between the excited singlet states in **FR0**. Although the calculated results do not take solvent H-bonding into account, the data are consistent with the hydrogen-bonding interactions between the solvent alcohol proton and the **FR0** carbonyl oxygen modulating the dipole moment in each excited state and thereby controlling the efficiency of solvent-solute dipole-dipole interactions. It is these interactions that appear to facilitate relaxation between the excited singlet states.

Conclusions

We have examined the excited state relaxation dynamics of the substituted fluorene derivative FR0. The experimental data in conjunction with the quantum chemical calculations reveal that relaxation between three excited singlet electronic states accounts for the spectral relaxation dynamics observed in protic solvents. The relaxation dynamics are related to the concentration of hydroxyl functionality in the solvent system, indicating that hydrogen bonding between the aldehyde oxygen of FR0 in the S₂ state and the solvent hydroxyl proton diminishes the role of dipolar solvent-solute coupling, reducing the relaxation rates for some of the relaxation pathways. Further experimentation will be required to address in detail the dependence of the electronic state coupling and its dependence on solvent interactions on chemical structure.

Acknowledgment

The collaboration between synthesis, theory, and experiments for the understanding and development of super photoreagents for precision chemistry is funded by a seed grant from DARPA and AMRDEC (W31P4Q-20-1-0001). Partial support comes from NIH (Grant Nos. 2R01EY016077-08A1 and 5R01EY025383-02 R01 to GJB, and R01GM101353 to BB), NSF

(Grant No. CHE1836498 to MD) and the U.S. DOE (Grant No. DE-FG02-01ER15228 to PP). This work was supported in part through computational resources and services provided by the Institute for Cyber-Enabled Research at Michigan State University. The views and conclusions contained in this document are those of the authors and should not be interpreted as representing the official policies, either expressed or implied, of the Defense Advanced Research Projects Agency, the U.S. Army, or the U.S. Government. The authors would like to thank Dr. Ilias Magoulas for providing the code used in generating the electronic density difference maps shown in this work.

References

- 1. Malval, J. P.; Diemer, V.; Savary, F. M.; Jacques, P.; Allonas, X.; Chaumeil, H.; Defoin, A.; Carré, C. Excited State Proton Transfer in a 'Super' Photoacid Based on a Phenol–Pyridinium Biaryl Chromophore. *Chem. Phys. Lett.* **2008**, *455* (4-6), 238-241.
- 2. Finkler, B.; Spies, C.; Vester, M.; Walte, F.; Omlor, K.; Riemann, I.; Zimmer, M.; Stracke, F.; Gerhards, M.; Jung, G. Highly Photostable "Super"-Photoacids for Ultrasensitive Fluorescence Spectroscopy. *Photochem. Photobiol. Sci.* **2014**, *13* (3), 548-562.
- 3. Sheng, W.; Nairat, M.; Pawlaczyk, P. D.; Mroczka, E.; Farris, B.; Pines, E.; Geiger, J. H.; Borhan, B.; Dantus, M. Ultrafast Dynamics of a "Super" Photobase. *Angew. Chem. Int. Ed.* **2018**, *57*, 14742-14746.
- 4. Lahiri, J.; Moemeni, M.; Kline, J.; Borhan, B.; Magoulas, I.; Yuwono, S. H.; Piecuch, P.; Jackson, J. E.; Dantus, M.;Blanchard, G. J. Proton Abstraction Mediates Interactions between the Super Photobase Fr0-Sb and Surrounding Alcohol Solvent. *J. Phys. Chem. B* **2019**, *123*, 8448-8456.
- 5. Lahiri, J.; Moemeni, M.; Magoulas, I.; Yuwono, S. H.; Kline, J.; Borhan, B.; Piecuch, P.; Jackson, J. E.; Blanchard, G. J.; Dantus, M. Steric Effects in Light-Induced Solvent Proton Abstraction. *Phys. Chem. Phys.* **2020**, *22* (35), 19613-19622.
- 6. Lahiri, J.; Moemeni, M.; Kline, J.; Magoulas, I.; Yuwono, S. H.; Laboe, M.; Shen, J.; Borhan, B.; Piecuch, P.; Jackson, J. E.; Blanchard, G. J.; Dantus, M. Isoenergetic Two-Photon Excitation Enhances Solvent-to-Solute Excited-State Proton Transfer. *J. Chem. Phys.* **2020**, *153* (22), 224301.
- 7. Kucherak, O. A.; Didier, P.; Mely, Y.; Klymchenko, A. S. Fluorene Analogues of Prodan with Superior Fluorescence Brightness and Solvatochromism. *J. Phys. Chem. Lett.* **2010,** *1*, 616-620.
- 8. Pillman, H. A.;Blanchard, G. J. Effects of Energy Dissipation on Motional Dynamics in Unilamellar Vesicles. *J. Phys. Chem. B* **2010**, *114*, 13703-13709.
- 9. Baumler, S. M. Diffusional Motion as a Gauge of Interfacial Fluidity and Adhesion of Supported Model Membrane Films. Ph.D. Dissertation, Michigan State University, East Lansing, MI, 2017.
- 10. Kohn, W.;Sham, L. J. Self-Consistent Equations Including Exchange and Correlation Effects. *Phys. Rev.* **1965**, *140*, A1133-A1138.
- 11. Hohenberg, P.;Kohn, W. Inhomogeneous Electron Gas. *Phys. Rev.* **1964**, *136*, B864-B871.
- 12. Yanai, T.; Tew, D. P.; Handy, N. C. A New Hybrid Exchange–Correlation Functional Using the Coulomb-Attenuating Method (Cam-B3lyp). *Chem. Phys. Lett.* **2004**, *393*, 51-57.

- 13. Hehre, W. J.; Ditchfield, R.;Pople, J. A. Self-Consistent Molecular Orbital Methods. Xii. Further Extensions of Gaussian-Type Basis Sets for Use in Molecular Orbital Studies of Organic Molecules. *J. Chem. Phys.* **1972**, *56*, 2257-2261.
- 14. Hariharan, P. C.; Pople, J. A. The Influence of Polarization Functions on Molecular Orbital Hydrogenation Energies. *Theor. Chim. Acta* **1973**, *28*, 213-222.
- 15. Clark, T.; Chandrasekhar, J.; Spitznagel, G. W.; Schleyer, P. v. R. Efficient Diffuse Function-Augmented Basis Sets for Anion Calculations. Iii. The 3-21+G Basis Set for First-Row Elements, Li–F. *J. Comp. Chem.* **1983**, *4*, 294-301.
- 16. Stanton, J. F.;Bartlett, R. J. The Equation of Motion Coupled-Cluster Method. A Systematic Biorthogonal Approach to Molecular Excitation Energies, Transition Probabilities, and Excited State Properties. *J. Chem. Phys.* **1993**, *98*, 7029-7039.
- 17. Čížek, J. On the Correlation Problem in Atomic and Molecular Systems. Calculation of Wavefunction Components in Ursell-Type Expansion Using Quantum-Field Theoretical Methods. *J. Chem. Phys.* **1966**, *45*, 4256-4266.
- 18. Purvis III, G. D.;Bartlett, R. J. A Full Coupled-Cluster Singles and Doubles Model: The Inclusion of Disconnected Triples. *J. Chem. Phys.* **1982**, *76* (4), 1910-1918.
- 19. Fradelos, G.; Lutz, J. J.; Wesołowski, T. A.; Piecuch, P.; Włoch, M. Embedding Vs Supermolecular Strategies in Evaluating the Hydrogen-Bonding-Induced Shifts of Excitation Energies. *J. Chem. Theory Comput.* **2011,** *7*, 1647-1666.
- 20. Gordon, M. S.; Schmidt, M. W., Advances in Electronic Structure Theory: Gamess a Decade Later. In *Theory and Applications of Computational Chemistry: The First Forty Years*, Dykstra, C. E.; Frenking, G.; Kim, K. S.; Scuseria, G. E., Eds. Elsevier: Amsterdam, 2005; pp 1167-1189.
- 21. Barca, G. M. J.; Bertoni, C.; Carrington, L.; Datta, D.; De Silva, N.; Deustua, J. E.; Fedorov, D. G.; Gour, J. R.; Gunina, A. O.; Guidez, E.; Harville, T.; Irle, S.; Ivanic, J.; Kowalski, K.; Leang, S. S.; Li, H.; Li, W.; Lutz, J. J.; Magoulas, I.; Mato, J.; Mironov, V.; Nakata, H.; Pham, B. Q.; Piecuch, P.; Poole, D.; Pruitt, S. R.; Rendell, A. P.; Roskop, L. B.; Ruedenberg, K.; Sattasathuchana, T.; Schmidt, M. W.; Shen, J.; Slipchenko, L.; Sosonkina, M.; Sundriyal, V.; Tiwari, A.; Vallejo, J. L. G.; Westheimer, B.; Włoch, M.; Xu, P.; Zahariev, F.;Gordon, M. S. Recent Developments in the General Atomic and Molecular Electronic Structure System. *J. Chem. Phys.* **2020**, *152* (15), 154102.
- 22. Piecuch, P.; Kucharski, S. A.; Kowalski, K.; Włoch, M. Efficient Computer Implementation of the Renormalized Coupled-Cluster Methods: The R-Ccsd[T], Rccsd(T), Cr-Ccsd[T], and Cr-Ccsd(T) Approaches. *Comp. Phys. Commun.* **2002**, *149*, 71-96.
- 23. Kowalski, K.;Piecuch, P. New Coupled-Cluster Methods with Singles, Doubles, and Noniterative Triples for High Accuracy Calculations of Excited Electronic States *J. Chem. Phys.* **2004**, *120*, 1715-1738.

- 24. Włoch, M.; Gour, J. R.; Kowalski, K.;Piecuch, P. Extension of Renormalized Coupled-Cluster Methods Including Triple Excitations to Excited Electronic States of Open-Shell Molecules *J. Chem. Phys.* **2005**, 214107.
- 25. Piecuch, P.; Gour, J. R.; Włoch, M. Left-Eigenstate Completely Renormalized Equation-of-Motion Coupled-Cluster Methods: Review of Key Concepts, Extension to Excited States of Open-Shell Systems, and Comparison with Electron-Attached and Ionized Approaches *Int. J. Quantum Chem.* **2009**, *109*, 3268-3304.
- 26. Humphrey, W.; Dalke, A.; Schulten, K. Vmd: Visual Molecular Dynamics. *J. Mol. Graphics* **1996**, *14*, 33-38.
- 27. Maroncelli, M.; Fleming, G. R. Picosecond Solvation Dynamics of Coumarin 153: The Importance of Molecular Aspects of Solvation. *J. Chem. Phys.* **1987**, *86*, 6221-6239.
- 28. Maroncelli, M.;Fleming, G. R. Comparison of Time-Resolved Fluorescence Stokes Shift Measurements to a Molecular Theory of Solvation Dynamics. *J. Chem. Phys.* **1988**, *89* (2), 875-881.
- 29. Nagarajan, V.; Brearley, A. M.; Kang, T. J.;Barbara, P. F. Time-Resolved Spectroscopic Measurements on Microscopic Solvation Dynamics. *J. Chem. Phys.* **1987**, *86*, 3183-3196.
- 30. Simon, J. D.;Su, S. G. Picosecond Stokes Shift Studies of Solvent Friction: Experimental Measurements of Time-Dependent Band Shape and Integrated Intensity. *Chem. Phys.* **1991**, *152*, 143-152.
- 31. Su, S. G.; Simon, J. D. Solvation Dynamics in Ethanol. *J. Phys. Chem* **1987**, *91*, 2693-2696.
- 32. Bagchi, B.; Oxtoby, D. W.; Fleming, G. R. Theory of the Time Development of the Stokes Shift in Polar Media. *Chem. Phys.* **1984**, *86*, 257-267.
- 33. Castner, J., E. W.; Maroncelli, M.; Fleming, G. R. Subpicosecond Resolution Studies of Solvation Dynamics in Polar Aprotic and Alcohol Solvents. *J. Chem. Phys.* **1987**, *86*, 1090-1097.
- 34. Castner, J., E. W.; Fleming, G. R.;Bagchi, B. Influence of Non-Debye Relaxation and of Molecular Shape on the Time Dependence of the Stokes Shift in Polar Media. *Chem. Phys. Lett.* **1988**, *143*, 270-276.
- 35. Eom, I.; Joo, T. Polar Solvation Dynamics of Coumarin 153 by Ultrafast Time-Resolved Fluorescence. *J. Chem. Phys.* **2009**, *131* (24), 244507.
- 36. Böhmer, R.; Gainaru, C.;Richert, R. Structure and Dynamics of Monohydroxy Alcohols—Milestones Towards Their Microscopic Understanding, 100 Years after Debye. *Phys. Rep.* **2014**, *545*, 125-195.
- 37. Eber, G.; Gruneis, F.; Schneider, S.; Dorr, F. Dual Fluorescence Emission of Azulene Derivatives in Solution. *Chem. Phys. Lett.* **1974**, *29*, 397-404.

- 38. Huppert, D.; Jortner, J.;Rentzepis, P. M. $S_2 \rightarrow S_1$ Emission of Azulene in Solution. *Chem. Phys. Lett.* **1972**, *13*, 225-228.
- 39. LeBel, R. G.; Goring, D. A. I. Density, Viscosity, Refractive Index, and Hygroscopicity of Mixtures of Water and Dimethyl Sulfoxide. *J. Chem. Eng. Data* **1962**, *7*, 100-101.
- 40. Mikhail, S. Z.; Kimel, W. R. Densities and Viscosities of 1-Propanol-Water Mixtures. *J. Chem. Eng. Data* **1963**, *8*, 323-328.

Table 1. The $S_0 \to S_n$ vertical excitation energies $\omega_n^{(EOMCC)}$ and the permanent dipole moments μ_n characterizing the lowest four singlet excited states, S_1 – S_4 , of FR0 in the gas phase.^a

State	$\omega_n^{(\text{EOMCC})}$ (eV)	μ_n (D)
S_1	3.56	15.2
S_2	3.81	2.5
S_3	3.95	10.0
S_4	4.27	7.8

^a The dipole moment of **FR0** in the ground S₀ state is 6.2 Debye.

Table 2. Transition dipole moments (TDM) and oscillator strengths (Osc. Str.) characterizing the electronic excitations to the lowest four excited singlet states of FR0 in the gas phase. Only $S_m \rightarrow S_n$ transitions with m < n are given in the Table.

Target	Initial state								
state	S_0		S_1		Sa	S_2		S_3	
	TDM (D)	Osc. Str.	TDM (D)	Osc. Str.	TDM (D)	Osc. Str.	TDM (D)	Osc. Str.	
S_1	7.5	0.84	_						
S_2	0.2	0.00	0.2	0.00		_			
S_3	2.9	0.14	3.4	0.02	0.1	0.00			
S ₄	0.5	0.00	0.2	0.00	0.0	0.00	0.8	0.00	

Table 3. Fitted rate constants for FR0 in *n*-propanol and *n*-pentanol.

Rate Constant and	Sol	vent
Associated Transition	<i>n</i> -propanol (× 10^9)	<i>n</i> -pentanol (× 10^9)
k_{32}	9.47 ± 1.02	9.02 ± 0.22
k_{31}	1.89 ± 1.10	1.70 ± 0.20
k_{30}	1.86 ± 0.63	4.21 ± 0.50
k_{21}	2.73 ± 0.62	0.40 ± 0.15
k_{20}	3.33 ± 0.81	0.23 ± 0.14
k_{10}	0.42 ± 0.05	0.84 ± 0.26

Table 4. Fitted rate constants for FR0 in *n*-propanol/DMSO binary solvent systems.

Rate Constant	Solvent					
and Associated	<i>n</i> -propanol	75% <i>n</i> -propanol	50% <i>n</i> -propanol	25% <i>n</i> -propanol		
Transition	$(\times 10^{9})$	$(\times 10^{9})$	$(\times 10^{9})$	$(\times 10^{9})$		
k ₃₂	9.47 ± 1.02	13.67 ± 0.26	14.64 ± 0.79	16.74 ± 1.04		
k_{31}	1.89 ± 1.10	4.10 ± 0.56	4.91 ± 0.36	5.31 ± 0.50		
k_{30}	1.86 ± 0.63	1.01 ± 0.34	1.76 ± 1.10	0.30 ± 0.36		
k_{21}	2.73 ± 0.62	2.80 ± 0.14	2.70 ± 0.16	2.60 ± 0.60		
k_{20}	3.33 ± 0.81	1.29 ± 0.13	0.80 ± 0.06	0.14 ± 0.13		
k_{10}	0.42 ± 0.05	0.36 ± 0.02	0.37 ± 0.01	0.32 ± 0.04		

Table 5. Fluorescence anisotropy and lifetime components for FR0 in n-propanol (PrOH), n-pentanol (PeOH), and DMSO. R(0) is the zero-time anisotropy and τ_{OR} is the orientational relaxation time constant.

λ (nm)	R(0)PrOH	τ _{OR-PrOH} (ps)	$R(0)_{ m PeOH}$	τ _{OR-PeOH} (ps)	$R(0)_{ m DMSO}$	τ _{OR-DMSO} (ps)
490	0.17 ± 0.05	271 ± 90	0.10 ± 0.03	491 ± 98	0.17 ± 0.02	242 ± 36
500	0.19 ± 0.02	400 ± 58	0.11 ± 0.01	788 ± 53	0.19 ± 0.01	331 ± 27
520	0.17 ± 0.01	610 ± 48	0.15 ± 0.01	941 ± 45	0.18 ± 0.01	309 ± 22
540	0.17 ± 0.01	571 ± 36	0.15 ± 0.01	1250 ± 43	0.19 ± 0.01	277 ± 19
560	0.18 ± 0.01	678 ± 40	0.19 ± 0.01	1489 ± 36	0.22 ± 0.01	319 ± 24
570	0.17 ± 0.01	734 ± 32	0.21 ± 0.01	1235 ± 29	0.21 ± 0.01	351 ± 28
580	0.19 ± 0.01	512 ± 19	0.21 ± 0.01	1057 ± 30	0.26 ± 0.03	319 ± 33
590	0.22 ± 0.01	518 ± 20	0.27 ± 0.01	1057 ± 29	0.36 ± 0.04	252 ± 26

Figure Captions

Figure 1. Molecular structures of (a) the FR0-SB Schiff base and (b) the FR0 precursor.

Figure 2. Time-resolved emission spectra of **FR0** in (a) *n*-propanol, (b) *n*-pentanol, and (c) DMSO extracted from experimental fluorescence lifetime data. The time corresponding to each spectrum are as follows: (—) 0 ps, (—) 50 ps, (—) 100 ps, (—) 200 ps, (—) 300 ps, (—) 400 ps, (—) 500 ps, (—) 750 ps, (—) 1000 ps, (—) 2000 ps, (—) 3000 ps, (—) 4000 ps, (—) 5000 ps, (—) 6000 ps, (—) 7000 ps, and (—) 8000 ps.

Figure 3. The structure of the isolated **FR0** chromophore in its ground electronic S_0 state and the computed Mulliken charges for selected atoms in the (a) S_0 , (b) S_1 , (c) S_2 , and (d) S_3 states of **FR0**.

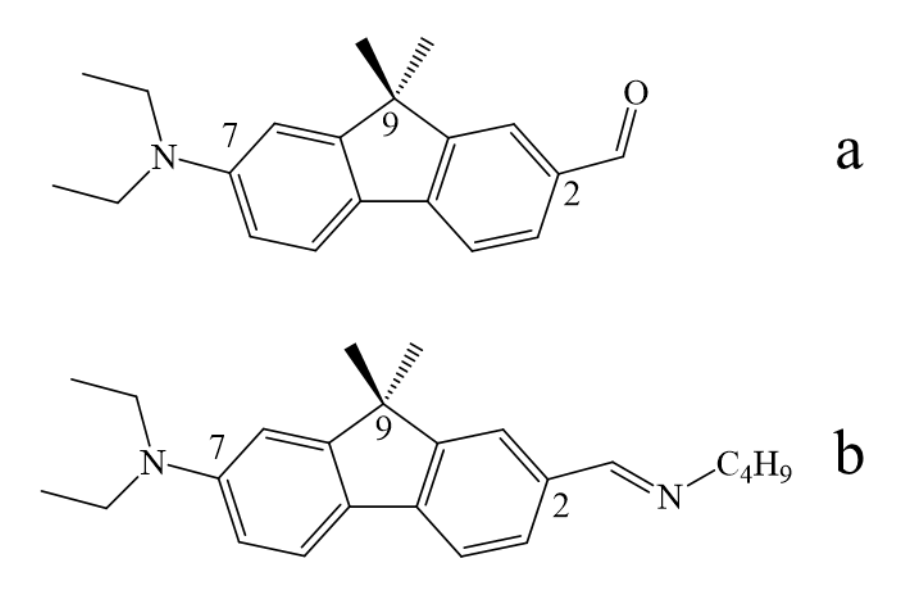
Figure 4. The structure of the isolated **FR0** molecule in its ground electronic S_0 state and the electronic density difference maps associated with the transition from S_0 to the (A) S_1 , (B) S_2 , and (C) S_3 states of **FR0**. The red/blue color indicates an increase/decrease in the electron density upon the $S_0 \rightarrow S_n$ (n = 1-3) excitation. The dipole moment vectors characterizing the S_0 (orange), S_1 (magenta), S_2 (green), and S_3 (cyan) states of **FR0** are shown as well.

Figure 5. Proposed kinetic model for the excitation and relaxation of **FR0** to the lowest three excited singlet states, in which k_{mn} denotes the rate constant associated with each $S_m \to S_n$ transition. Dashed arrows represent radiative decays and solid arrows represent non-radiative decays.

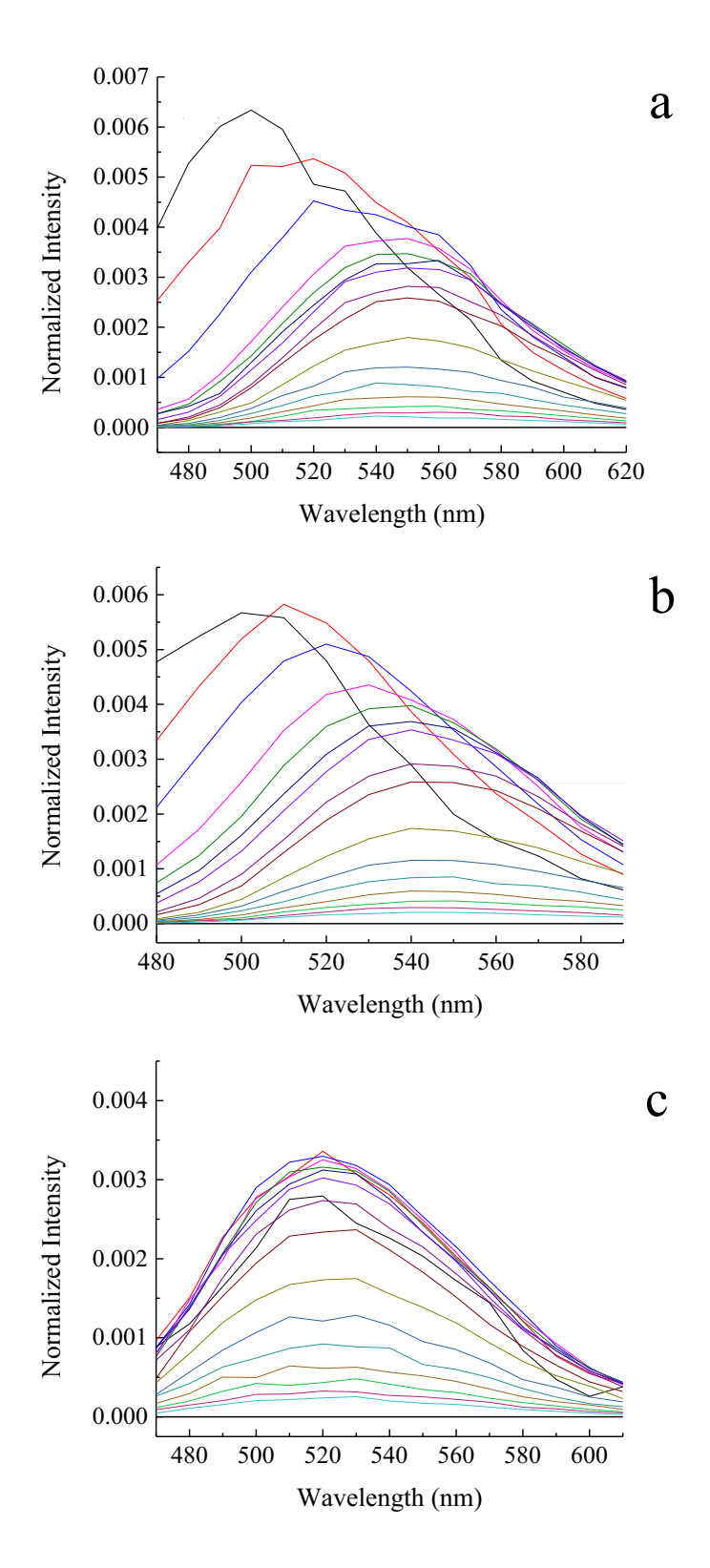
Figure 6. Steady-state fluorescence emission spectra of **FR0** in (a) *n*-propanol (PrOH), (b) *n*-pentanol (PeOH), and (c) DMSO in the frequency domain fit to three Gaussian bands. In each spectrum, the identity of each band is as indicated: (—) ss emission (unresolved), (—) $S_1 \rightarrow S_0$ emission, (—) $S_2 \rightarrow S_0$ emission, and (—) $S_3 \rightarrow S_0$ emission.

Figure 7. Normalized intensities of the three fitted bands (spectral features) extracted from the normalized time-domain data as a function of time for **FR0** in (a) *n*-propanol and (b) *n*-pentanol. The spectral features are as indicated: (—) $S_3 \rightarrow S_0$, (—) $S_2 \rightarrow S_0$, and (—) $S_1 \rightarrow S_0$.

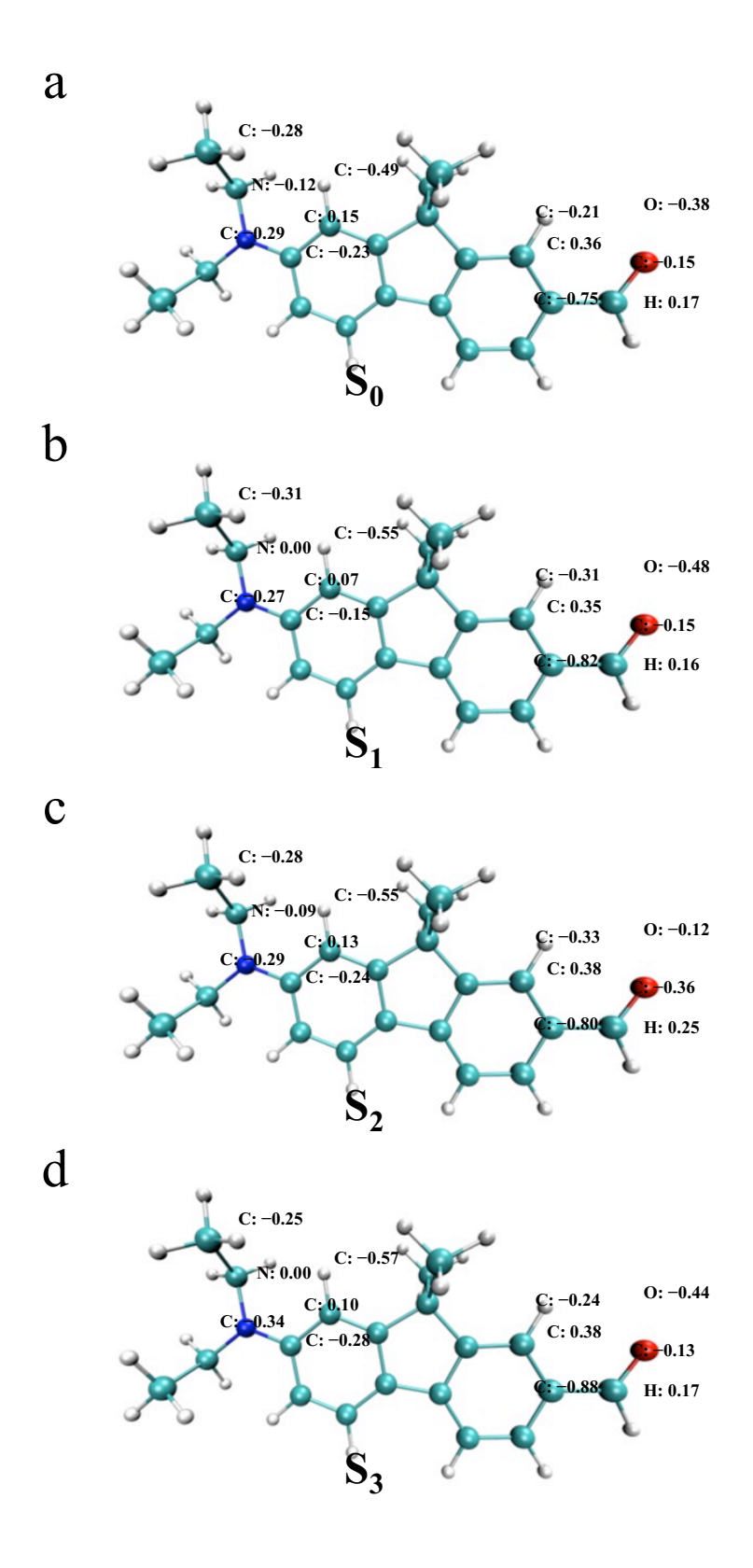
Figure 8. Fitted rate constants for **FR0** in *n*-propanol/DMSO binary mixture as a function of percent *n*-propanol present.



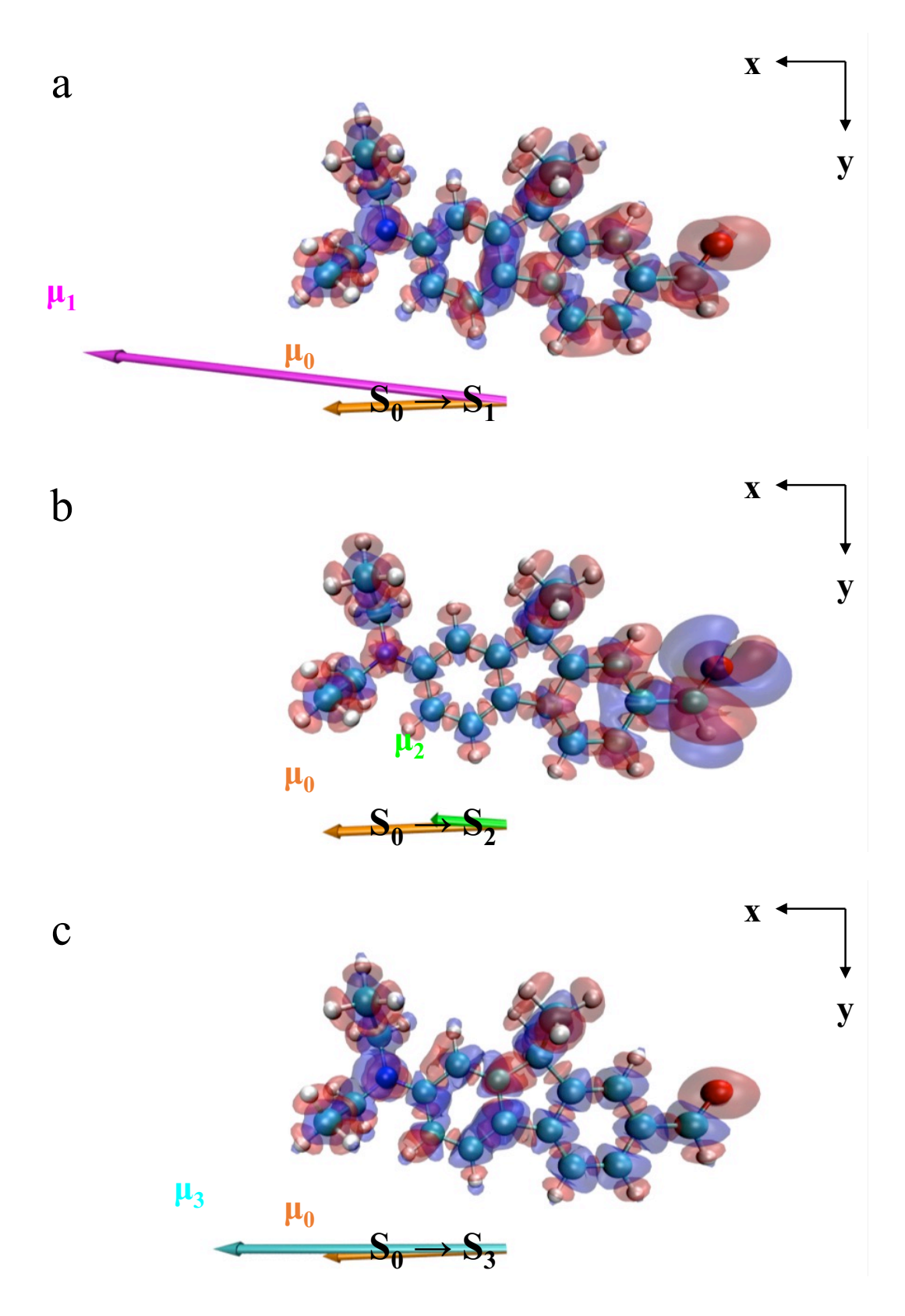
Capistran et al. Figure 1



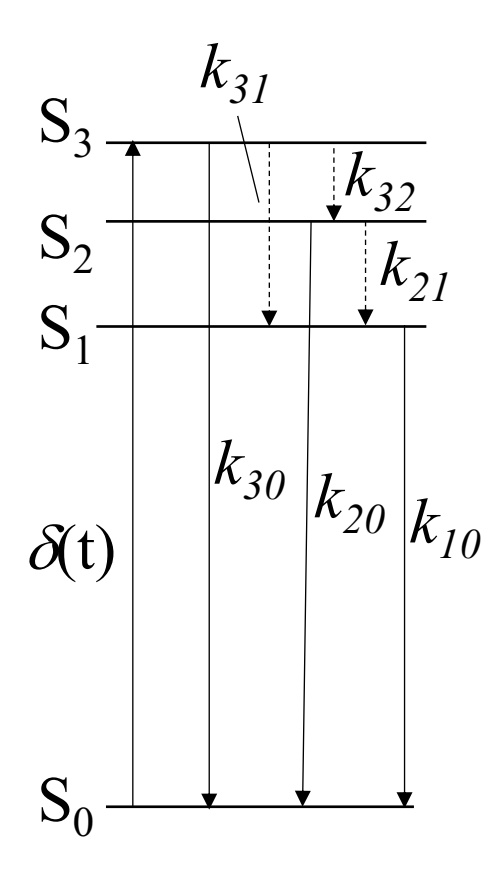
Capistran et al. Figure 2



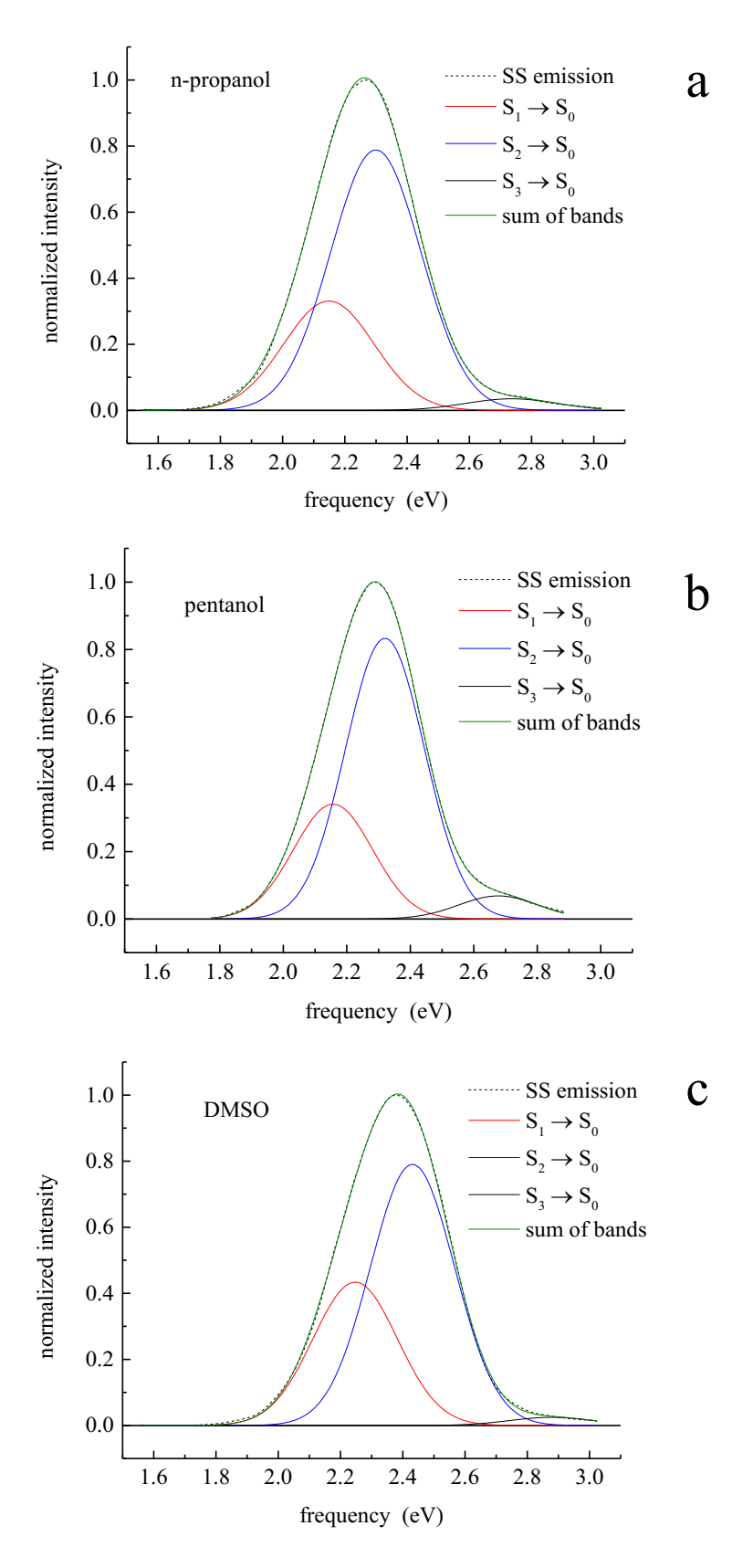
Capistran et al. Figure 3



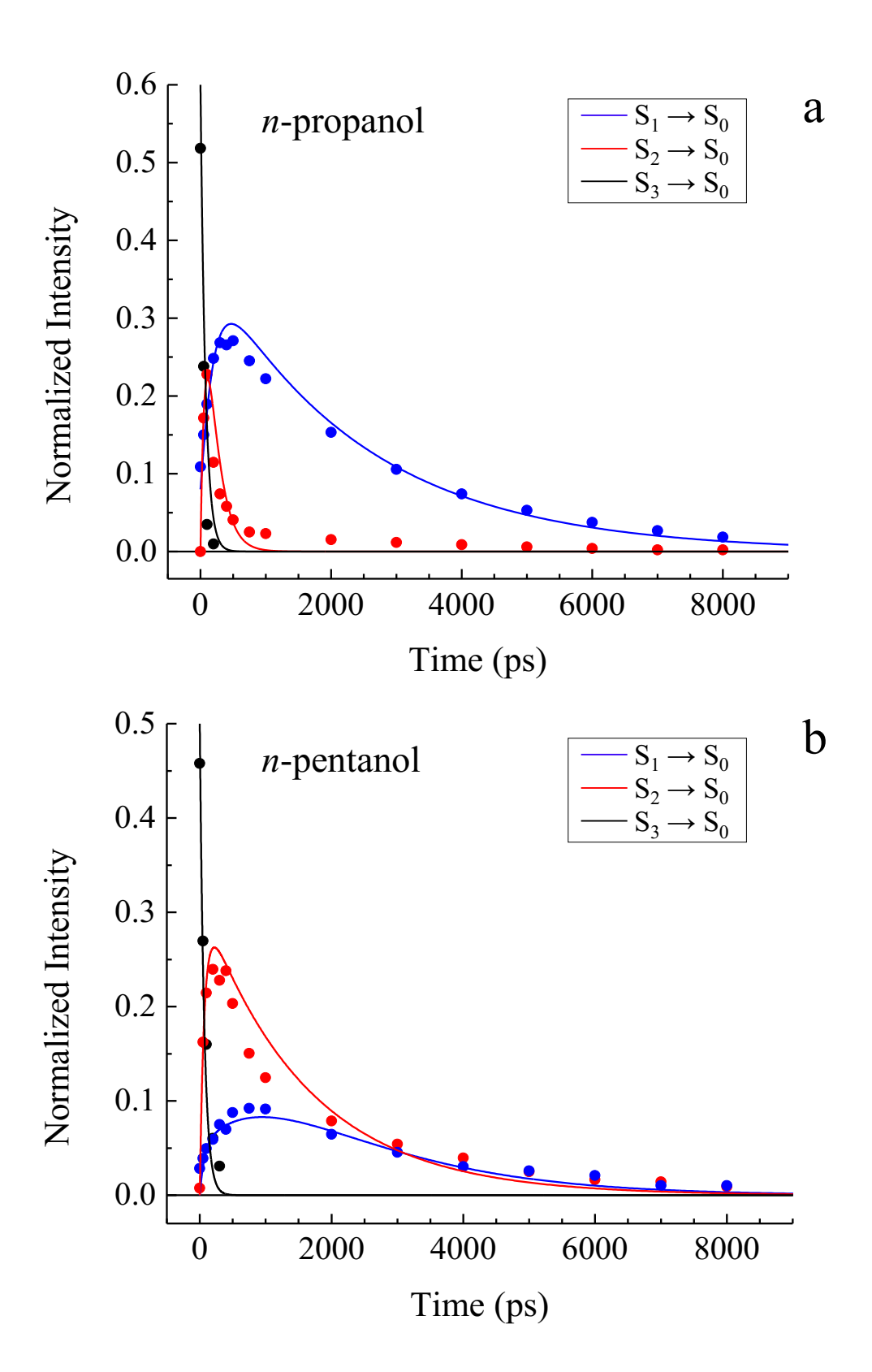
Capistran et al. Figure 4



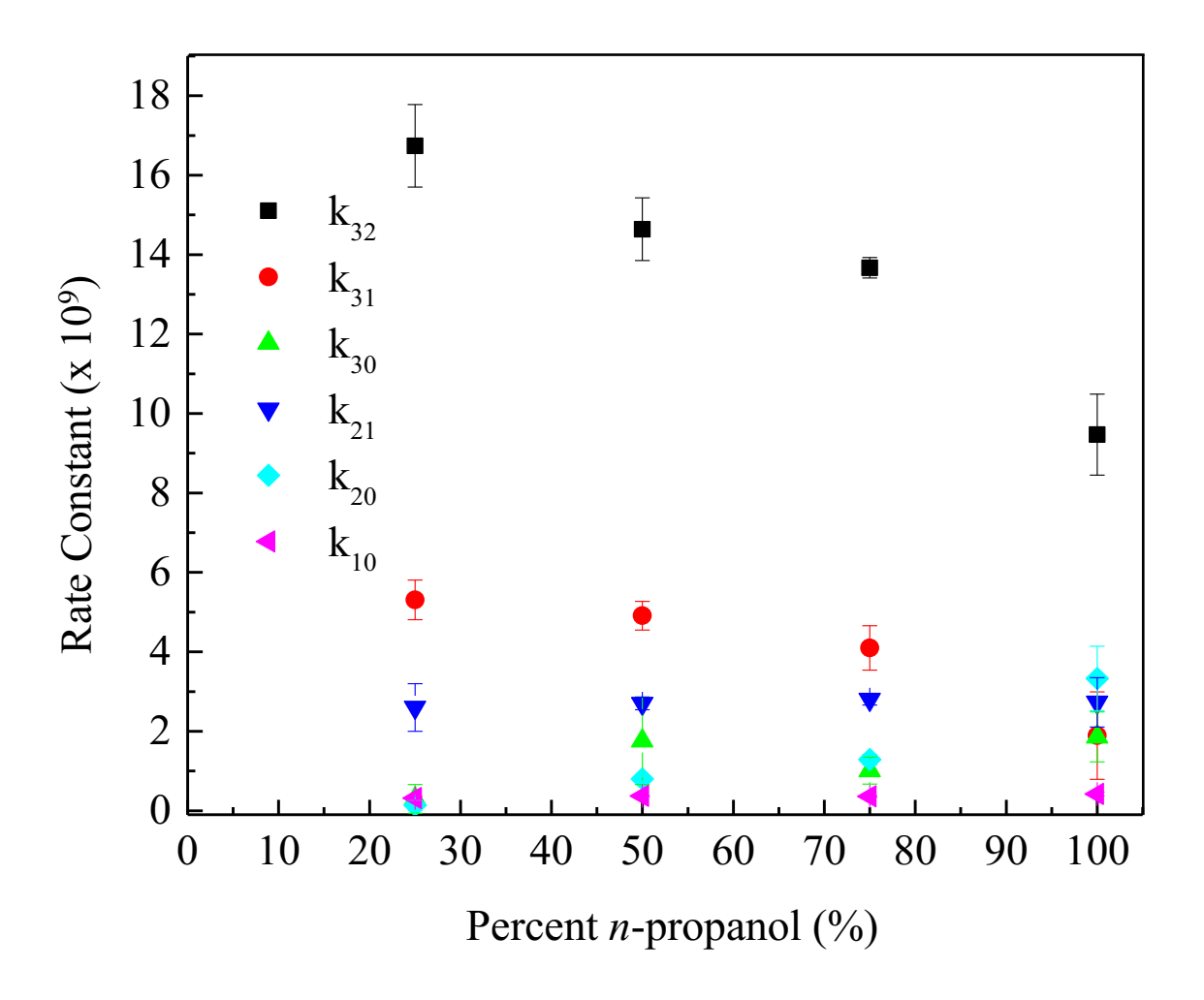
Capistran et al. Figure 5



Capistran et al. Figure 6



Capistran et al. Figure 7



Capistran et al. Figure 8